JOURNAL OF AIRCRAFT
Vol. 12, No. 4, July–August 1996

Aeroelastic Optimization of a Helicopter Rotor to Reduce Vibration and Dynamic Stresses

Ranjan Ganguli* and Inderjit Chopra†
University of Maryland, College Park, Maryland 20742

Optimization studies are carried out for a four-bladed, soft in-plane hingeless rotor consisting of a two-cell composite box–beam spar. The design variables are the ply angles of the box–beam walls. The objective functions are the vibratory hub loads and the vibratory blade bending moments; constraints are imposed on blade rotating frequencies and aeroelastic stability. The objective functions are first minimized individually, and then a combined optimization is performed to minimize both the objectives simultaneously. As compared to the starting design, the optimum solution results in a 15–60% reduction of the 4/rev hub loads as well as a reduction in the peak-to-peak flap and lag bending moments of 11 and 14%, respectively. Starting from an initially infeasible starting design with a 3% requirement on lag mode damping, the optimum solution with composite chordwise bending–torsion coupling results in an increase in lag mode damping of over 200% compared to the starting design.

Nomenclature

C_T	= thrust coefficient
c	= blade chord
D_j	= blade section properties
EA, EI_y, EI_z	= blade axial, flap bending, and lag bending stiffness
F^{4P}_{xH}, F^{4P}_{yH}, F^{4P}_{zH}	= 4/rev longitudinal, lateral, and vertical force
GJ	= blade torsional stiffness
g	= constraints
J, J_d, J_v	= combined objective function, objective function for dynamic stress, and objective function for vibration
$\bar{k}_{23}$, $\bar{k}_{24}$	= blade flap and lag bending–torsion coupling
M^{jP}_{xR}, M^{jP}_{yR}, M^{jP}_{zR}	= j/rev torsion, flap bending, and lag bending moment
M^{4P}_{xH}, M^{4P}_{yH}, M^{4P}_{zH}	= 4/rev rolling, pitching, and yawing moment
m_0	= reference mass per unit length
N	= number of beam finite elements, number of blades
R	= rotor radius
T	= kinetic energy
U	= strain energy
u_e, v, w	= axial, lag, and flap deformation of blade
W	= virtual work
Y	= blade response
α_k	= real part of characteristic exponent of kth mode
β	= flap angle
δ	= variation
ε_k	= minimum acceptable level of damping for kth mode
ζ	= lag angle
θ	= ply angle design variables
μ	= advance ratio
σ	= solidity ratio
Φ	= mode shape
ϕ	= torsional deformation of blade
ψ	= azimuth angle, time
Ω	= rotation speed
ω	= blade rotating frequencies

Presented in part as Paper 94-1420 at the AIAA 35th Structures, Structural Dynamics, and Materials Conference, Hilton Head, SC, April 18–20, 1994; received Jan. 28, 1995; revision received Oct. 21, 1995; accepted for publication Feb. 14, 1996.

*Assistant Research Scientist, Center for Rotorcraft Education and Research, Department of Aerospace Engineering. Member AIAA.

†Professor and Director, Center for Rotorcraft Education and Research, Department of Aerospace Engineering. Fellow AIAA.

Introduction

SUPERIOR fatigue characteristics and a high stiffness–weight ratio compared to metals has resulted in widespread use of composite materials in the design of helicopter blades. Other potential benefits of composites such as their flexibility in tailoring structural characteristics have not yet been exploited by the rotorcraft industry. Selected studies have shown that composite couplings can reduce helicopter vibrations, enhance blade stability, and reduce blade stresses.[1,2] However, there are conflicting influences of the composite couplings on various rotor system characteristics, which can complicate the design process. Addressing this issue, optimization methods are applied in this article to minimize vibration and blade dynamic stresses, and enhance aeroelastic stability, by tailoring helicopter blade composite couplings.

High vibrations and high blade dynamic stresses in helicopters are caused by harmonic loading on the rotor caused by an unsteady aerodynamic environment and highly flexible rotating blades. For example, for a rotor with N blades, the N/rev forces and moments are transmitted by the rotor to the fuselage as a primary source of vibration. A direct approach for reducing these vibrations is to design the rotor to produce low vibratory hub loads. Also, vibratory bending moments acting along the blade length cause dynamic stresses, at several harmonics, on the rotor blade. These dynamic stresses cause structural fatigue, leading to a reduction in blade life. The critical dynamic stresses generally occur at the spanwise location where the vibratory bending moment is highest; for hingeless rotors this occurs at the blade root and for articulated rotors around the blade midsection. Therefore, a direct approach for increasing the life of a blade is to design the rotor to produce low vibratory bending and torsional moments at the critical spanwise locations. To design rotors with low vibration, considerable research has been directed towards the application of aeroelastic optimization methodology.[3]

Early studies on aeroelastic optimization of helicopter rotors focused on metal blades.[3] Addressing this issue, the authors[4,5] carried out an aeroelastic optimization study for a hingeless composite rotor with blade spar modeled as a box–beam.[6] Design variables were the ply angles of the box–beam, and the objective function was a combination of the vibratory hub loads. Constraints were imposed on blade frequencies and aeroelastic stability. Optimization was performed for several layups and configurations. It was found that elastic stiffnesses reduce the vibratory hub loads by about 20–40%; composite couplings yield a further reduction of about 10–15%.

Attempts to minimize vibration alone, such as those discussed previously, may cause an increase in the dynamic stresses. For example, minimizing the 4/rev hub loads for a 4-bladed hingeless rotor in forward flight, can result in an increase in the 1/rev, 2/rev and 6/rev blade root bending moments, causing higher dynamic stresses.[5] Selected studies have addressed the issue of reducing blade dynamic stresses. Peters and Cheng[7] used a frequency placement approach to satisfy stress constraints on the rotor blade. By keeping the blade bending and torsion natural frequencies away from harmonics of the rotor speed, resonant amplification of the blade response caused from the periodic aerodynamic forcing was avoided. In another study, Banerjee and Shanthakumaran[8] applied optimization methodology to the design of the flexbeam of a bearingless rotor to minimize the peak combined stresses along the flexbeam length to reduce fatigue loads. Their results showed a 70% reduction of the combined peak normal stress. These studies highlighted the need for using dynamic stresses as constraints, but were limited in their modeling of aeroelastic interactions. However, it is well established that aeroelastic couplings have considerable influence on blade harmonic loading. Hence, there is a need to use comprehensive aeroelastic optimization methodology to minimize the source of the blade dynamic stresses: the first few harmonics of the bending moments.

In this article, an objective function is developed to reduce both vibration (using vibratory hub loads) and dynamic stresses (using vibratory bending moments) at the blade root. Using suitable weighting functions in the objective function, aeroelastic optimization for a composite rotor blade with aeroelastic tailoring is performed for minimizing 1) vibratory hub loads, 2) vibratory blade bending moments, and 3) vibratory hub loads and blade bending moments.

Formulation

The aeroelastic and sensitivity analysis are based on a finite element method in space and time and are discussed in Refs. 4 and 5, respectively. Three different objective functions are used in this study. The first represents the vibratory hub loads J_v alone, the second represents the vibratory blade bending and torsional moments J_d, and the third represents a combination of both the vibratory hub loads and blade bending moments J. Ply angles θ_i of the walls of the two-cell box–beam spar are used as design variables.

The first type of objective function J_v is a sum of the scalar norms of the N/rev forces and the N/rev moments transmitted by an N-bladed helicopter rotor to the fuselage as a primary source of vibration and is defined as

$$J_v = \sqrt{(F_{xF}^{NP})^2 + (F_{yF}^{NP})^2 + (F_{zF}^{NP})^2} + \sqrt{(M_{xF}^{NP})^2 + (M_{yF}^{NP})^2 + (M_{zF}^{NP})^2} \quad (1)$$

where the forces and moments are nondimensionalized with respect to $m_0\Omega^2R^2$ and $m_0\Omega^2R^3$, respectively. The second type of objective function J_d is a measure of the vibratory bending and torsional moments at the blade root that is the source of dynamic stresses for a hingeless rotor and is defined as

$$J_d = \sum_{j=1}^{M=6} j\sqrt{(M_{xR}^{jP})^2 + (M_{yR}^{jP})^2 + (M_{zR}^{jP})^2} \quad (2)$$

Again, the vibratory bending moments in J_d are nondimensionalized by dividing by $m_0\Omega^2R^3$. This function is the weighted norm of the first M harmonics of the blade root bending and torsional moments. The number M is selected as six for this study, since it is found that six harmonics provide an accurate representation of the blade root bending moment. In general, the 1/rev bending moment is the largest in magnitude and the higher harmonic components become smaller. To increase the weight of the higher harmonics (2/rev, 3/rev, . . . , M/rev) in J_d, the jth harmonic component of the objective is multiplied by the number j. For the combined optimization, J is defined using the function scalarization approach:

$$J = K_1J_v + K_2J_d \quad (3)$$

Defining $K_1 + K_2 = 1$, we observe that when $K_1 = 0$, $J = J_d$ and when $K_2 = 0$, $J = J_v$. To give equal weight to both components of the objective function, K_1 and K_2 are chosen by solving the following equations: $K_1J_v = K_2J_d$ and $K_1 + K_2 = 1$. These two equations ensure equal weights for the values of the two components of the objective function. Solving these equations for K_1 and K_2, and substituting these in Eq. (3) yields the combined objective function:

$$J = 2J_vJ_d/(J_v + J_d) \quad (4)$$

Constraints are imposed on 1) aeroelastic stability and 2) frequency placement. The aeroelastic stability constraint keeps the rotor blade stable at the flight condition and is expressed as $g_s(\theta) = \alpha_k + \varepsilon_k \leq 0$ for the kth mode. The frequency placement constraint prevents blade resonance at frequencies not covered by the objective function, and are expressed as $g_f^L(\theta) = 1 - \omega_k/\omega_k^L \leq 0$ and $g_f^U(\theta) = 1 - \omega_k/\omega_k^U \geq 0$ for the kth mode.

Results and Discussion

For the numerical study, a four-bladed, soft in-plane hingeless composite rotor is considered. The rotor properties are given in Table 1. For the analysis, the blade is divided into five equally spaced finite elements. For discretization in the time domain, four temporal finite elements with quartic polynomial distribution within each element are used. Eight normal modes (three flap, two lag, two torsion, and one axial) are used for the trim analysis, and seven modes (three flap, two lag, and two torsion) are used for the stability analysis. Results are obtained at a forward speed of $\mu = 0.3$ and a C_T/σ of 0.07.

The blade spar is modeled as a two-cell box–beam made of graphite/epoxy (AS4/3501-6) plies. The box–beam has an outer box width of 4.2 in. and an outer box height of 2.2 in. (Fig. 1a). Each wall of the box–beam has 26 plies, each having a thickness of 0.005 in. Ply elastic stiffness properties are E_L = 20.59 msi, E_T = 1.42 msi, G_{LT} = 0.87 msi, and ν_{LT} = 0.42 msi. By choosing different ply layups, selected couplings can be introduced (Fig. 1b). The configuration consisting of balanced laminates with no elastic couplings is designated as uncoupled A. The symmetric A layup with unbalance in the horizontal walls has flap bending–torsion couplings. The symmetric D layup with unbalance in the vertical walls has

Table 1 Rotor properties

Number of blades, 4
Radius, 16.2 ft
Hover tip speed, 650 ft/s
C_l, 5.73α
C_d, $0.0095 + 0.2\alpha^2$
C_m, 0.0
c/R, 0.08
σ, 0.10
Precone β_p, 0.0
Lock number γ, 6.34
Mass per unit length, m_0, 0.135 slug/ft

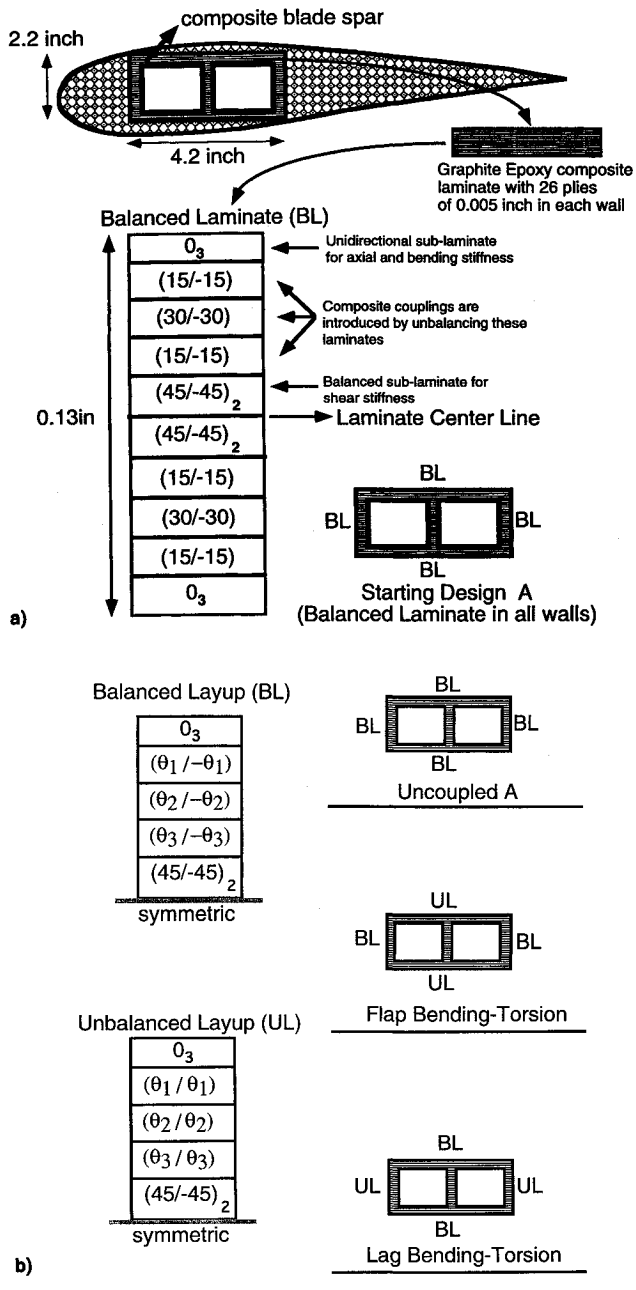

Fig. 1 a) Cross-sectional dimensions of the two-cell box–beam blade spar and baseline laminate and b) uncoupled and coupled layups used for the optimization study.

lag bending–torsion coupling. The signs of the coupling depend on the values of the design variables θ_1, θ_2, and θ_3.

Aeroelastic optimization is performed for three cases. For case 1, the objective is to minimize the 4/rev vibratory hub loads using the objective function J_v. For case 2, the objective is to minimize the first six harmonics of the vibratory bending and torsional moments using the objective function J_d. Finally, case 3 involves the minimization of both the 4/rev hub loads and the harmonics of the vibratory bending and torsional moments using the combined objective function J. The ply angles θ are allowed complete freedom to move in the design space; the optimizer can therefore select the desired sign of the coupling at any spanwise station. The upper and lower bounds on the blade frequencies are $0.60/\text{rev} \leq \omega_{1L} \leq 0.80/\text{rev}$, $1.08/\text{rev} \leq \omega_{1F} \leq 1.18/\text{rev}$, and $2.50/\text{rev} \leq \omega_{1T} \leq 6.50/\text{rev}$, where the subscripts $1L$, $1F$, and $1T$ denote the first lag, flap, and torsion modes, respectively. For the stability constraint, ε_k is chosen to be zero. The stability constraint is applied on the first flap, lag, and torsion modes. The optimization study is conducted using the optimizer CONMIN (Ref. 9).

Case 1: Minimization of Vibratory Hub Loads

The optimization is first performed for the uncoupled A layup. For the starting design, the design variables are θ_1^i = 15 deg, θ_2^i = 30 deg, and θ_3^i = 15 deg (Fig. 1a). This starting design (called starting design A) is feasible and the optimizer shows good convergence characteristics when starting from this design. All optimization cases in this article are started from the starting design A. For the uncoupled A layup, J_v is reduced by 23% compared to the starting design (Fig. 2). This reduction in the vibratory hub loads is from elastic stiffnesses only. Next, optimization is performed for the symmetric A and D layups. Compared to the uncoupled A optimum design, there is a further reduction in J_v of 16% for the symmetric A layup and a small reduction of about 3% for the symmetric D layup (not shown). This shows that the lag bending–torsion coupling has a minor influence on vibratory hub loads. Note that the symmetric D-I design shown in the figures is for an initially infeasible design that is discussed later.

It is clear that elastic stiffness and couplings can be used to obtain considerable reduction in the vibratory hub loads (Figs. 3 and 4). Comparing the symmetric A optimum design to the starting design A shows a reduction in the 4/rev longitudinal, lateral, and vertical forces of about 20% each, and a reduction in the rolling, pitching, and yawing moment of about 30, 35, and 70%, respectively.

The flap, lag, and torsion stiffness distributions along the blade span, for the starting and the optimum designs, are shown in Figs. 5, 6, and 7, respectively, where they are nor-

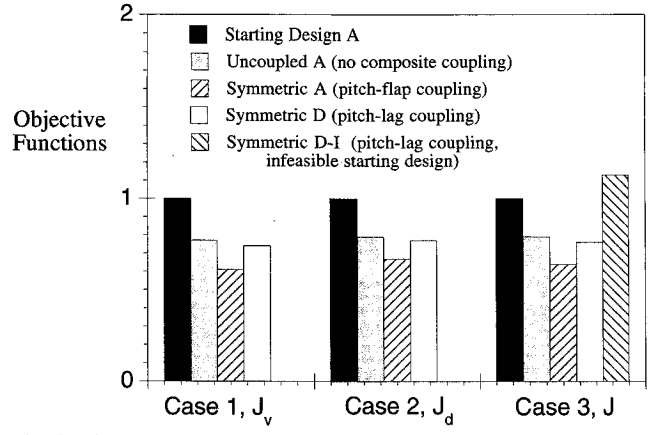

Fig. 2 Objective function corresponding to initial and optimum designs, normalized with starting design A values.

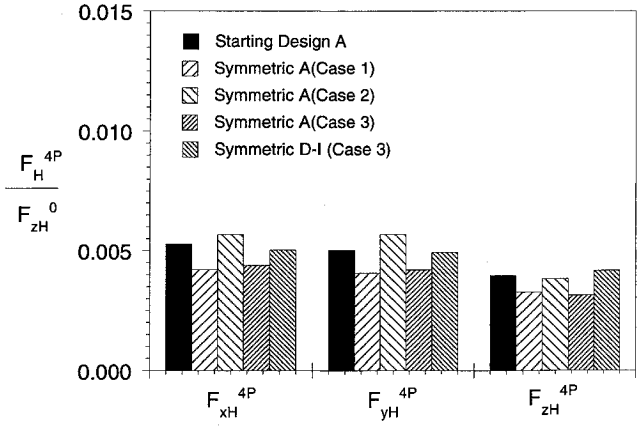

Fig. 3 Vibratory hub forces corresponding to initial and optimum designs, normalized by steady thrust.

malized with the starting design values. The starting design A is uniform and has flap, lag, and torsional stiffness of EI_y = 0.0079, EI_z = 0.0205, and GJ = 0.0023, respectively, and has no elastic couplings. The values of elastic stiffness in these figures can be interpreted as percentage changes from starting design A. The symmetric A optimum designs are stiffer in flap and lag and softer in torsion, compared to the starting design. The spanwise distributions of the flap bending–torsion and lag bending–torsion coupling are shown in Fig. 8. For the symmetric A optimum, the flap bending–torsion coupling $\bar{k}_{23}$ is positive in sign and is distributed throughout the blade span. The coupling is maximum at the root, decreases slightly at the midsection, and again increases at the tip. The variation of the ply angle design variables along the bladespan for the starting and optimum designs is shown in Figs. 9–11. For the symmetric A optimum design, the ply angles are between 0–30 deg. This may be because the largest composite couplings are obtained within this range. The ply angles are rounded off to the nearest integer values. The results for the optimum designs are obtained by running the aeroelastic analysis using these integer ply angles.

Figure 12 shows the damping of the first lag, flap, and torsion modes for several different layups normalized with starting design A values: σ_L = 0.0099, σ_F = 0.488, and σ_T = 0.932. The flap and torsion modes are highly damped and the lag mode is low damped. The symmetric A optimum design shows

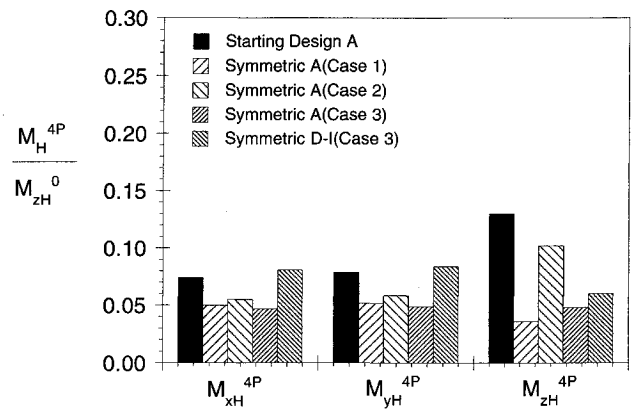

Fig. 4 Vibratory hub moments corresponding to initial and optimum designs, normalized by steady yawing moment.

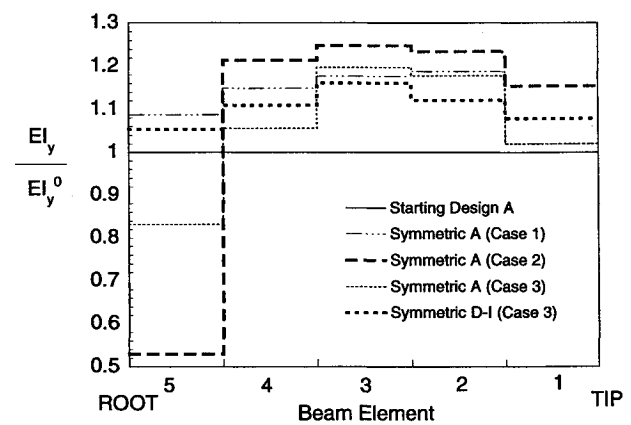

Fig. 5 Spanwise distribution of flap stiffness, normalized with starting design A values.

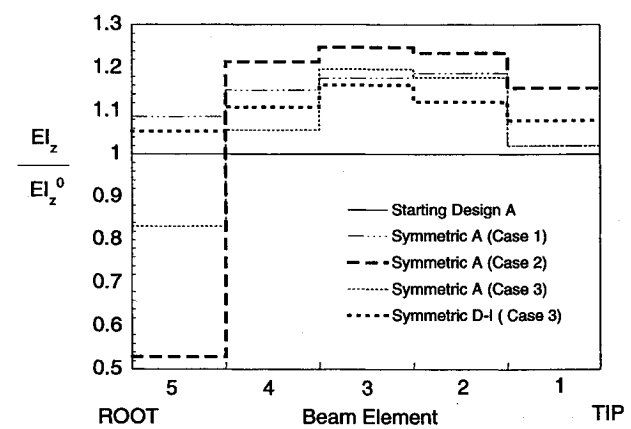

Fig. 6 Spanwise distribution of lag stiffness, normalized with starting design A values.

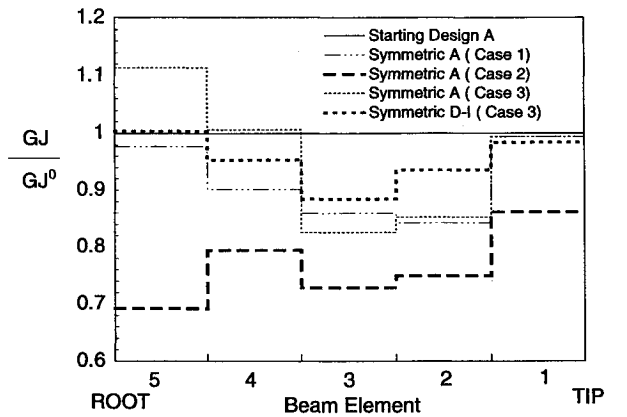

Fig. 7 Spanwise distribution of torsion stiffness, normalized with starting design A values.

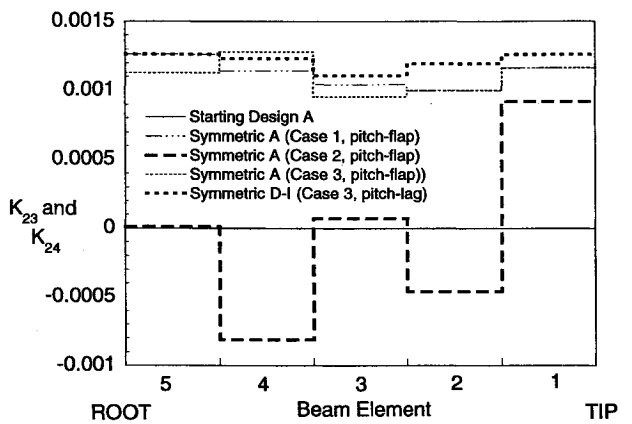

Fig. 8 Spanwise distribution of bending–torsion coupling for the coupled optimum design.

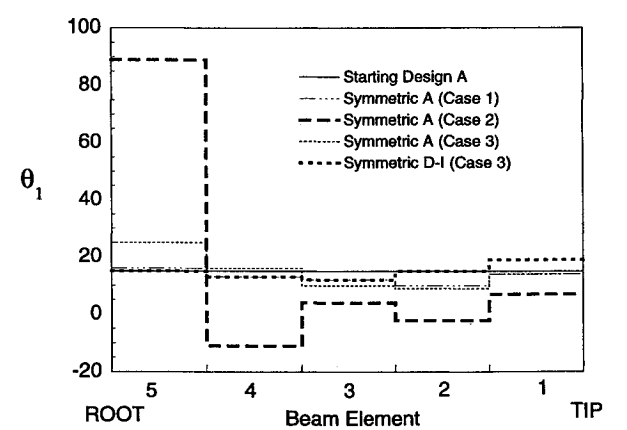

Fig. 9 Spanwise distribution of θ_1 for initial and optimum designs.

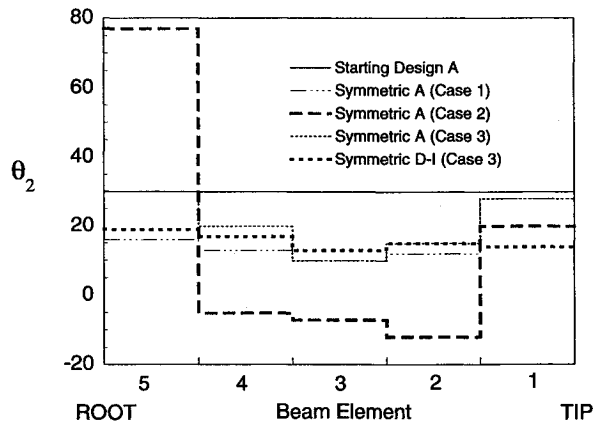

Fig. 10 Spanwise distribution of θ_2 for initial and optimum designs.

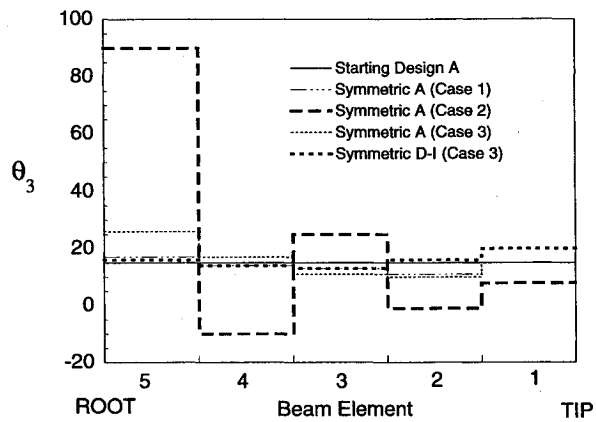

Fig. 11 Spanwise distribution of θ_3 for initial and optimum designs.

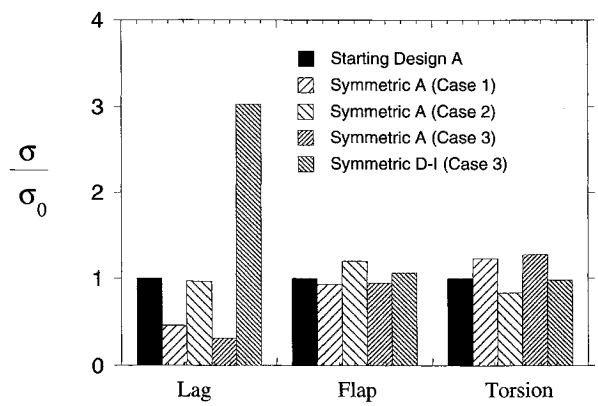

Fig. 12 Damping of first lag, flap, and torsion modes for the initial and optimum designs, normalized by starting design A values.

a decrease in the flap and lag mode damping, and an increase in the torsion mode damping.

The significant reductions in the 4/rev hub loads comes at the expense of the vibratory bending moments at the blade root. This is clear from Figs. 13 and 14, which show the first six harmonics of the flapwise moment M_y and the lagwise moment M_z at the blade root. The torsional moment M_x is an order of magnitude smaller than the bending moments and is therefore not presented. All of the harmonics are normalized with starting design A values, and so the changes in the harmonics can be interpreted as percentage changes from the starting design. Comparing the results of the starting design A and the symmetric A optimum configurations shows a reduction in the

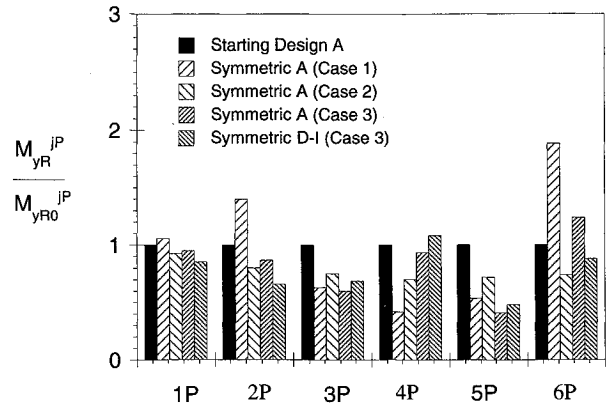

Fig. 13 Harmonics of vibratory flap bending moment at the blade root corresponding to the initial and optimum designs, normalized by starting design A values.

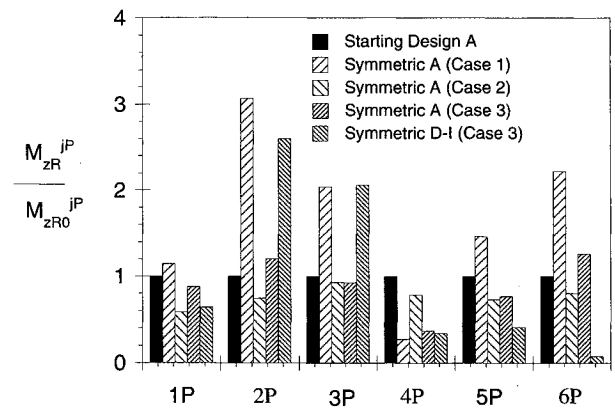

Fig. 14 Harmonics of vibratory lag bending moment at the blade root corresponding to the initial and optimum designs, normalized by starting design A values.

3, 4, and 5/rev blade root loads. This is because minimizing the 4/rev loads in the fixed frame requires that the 3, 4, and 5/rev loads are reduced in the rotating frame. However, this comes at the expense of an increase in the 1/rev, 2/rev, and 6/rev loads, which are not covered by the objective function. In fact, compared to the starting design A, there is an increase in the peak-to-peak flap and lag bending moment of 17 and 12%, respectively. These vibratory bending moments cause an increase in the dynamic stresses for the optimum blade, resulting in reduced fatigue life.

Case 2: Minimization of Vibratory Bending Moments

To reduce the vibratory bending moments at the blade root, the objective function J_d is minimized. Performing optimization on the uncoupled A layup yields a reduction in J_d of 21% compared to the starting design A (Fig. 2). Next, the optimization is performed for the coupled layups. Compared to the uncoupled A layup, the symmetric A and D layups show a further decrease in J_d of 12 and 2%, respectively. It appears that lag bending–torsion coupling is not useful for reducing the vibratory bending moments.

The symmetric A layup shows a reduction in the objective J_d of 33% from the starting design A. Figures 13 and 14 show that all six harmonics of the vibratory flap and lag bending moments are reduced. For the flap moment, the first six harmonics are reduced by 10, 20, 25, 30, 25, and 25%, respectively, and for the lag moment the reductions are 40, 30, 10, 20, 25, and 20%, respectively. The peak-to-peak flap and lag vibratory bending moments are reduced by 13 and 40%, respectively, compared to the starting design. Since the vibratory bending moments are dominated by the lag moment, the 40%

reduction in its peak-to-peak value can lead to a considerable decrease in the blade root dynamic stresses.

To investigate the causes for the reduction in the vibratory bending moments, we look at the elastic stiffnesses and couplings (Figs. 5–8). For the symmetric A layups, there is a reduction in the flap and lag stiffness at the blade root of about 50% each and an increase at the outboard elements of about 5–20%. The torsional stiffness decreases throughout the blade span and by about 30% at the blade root. It is clear that the decrease in the vibratory bending moments is obtained by making the inboard element much more flexible compared to the starting design. The symmetric A layup shows a distribution of flap bending–torsion coupling along the blade span with positive coupling in the first, third, and fifth elements, and negative coupling at the second and fourth elements. The variation of the ply angle design variables along the blade span for the symmetric A optimum design is shown in Figs. 9–11. At the root element, the ply angles are increased to high values (60–90 deg); this causes the large reduction of flexural stiffness for the case 2 optimum designs.

The damping for different layups is shown in Fig. 12. The symmetric A optimum designs show a decrease in the lag and torsion mode damping and an increase in flap mode damping. Again, the stability constraint does not become active during the optimization process.

From Figs. 3 and 4, it can be seen that the reduction in the vibratory bending moments comes at the expense of the 4/rev hub loads. In fact, comparing the symmetric A optimum to the starting design A shows an increase in the 4/rev longitudinal and lateral forces of about 10%. The 4/rev rolling moment is reduced by about 25% and the 4/rev pitching and yawing moments are decreased by about 20% each. The 4/rev vertical shear remains almost unchanged from the starting design value. The decrease in the 4/rev moments can be attributed to the reduction in all harmonics of the bending moments at the blade root for these optimum designs. However, this decrease in 4/rev moments is smaller than that obtained for the case 1 design where only the 4/rev hub loads were minimized.

Case 3: Combined Optimization

The previous results show that vibratory hub loads as well as blade root bending moments can be reduced by tailoring the structural properties of the blade. However, the reduction in vibratory hub loads is accompanied by an increase in blade bending moments, and the opposite happens when the blade bending moments are minimized. To investigate whether it is possible to minimize both the vibratory hub loads and the bending moments simultaneously, the combined objective function J is minimized.

Optimization is first performed for the uncoupled A layup. There is a reduction in J of 21%, compared to starting design A (Fig. 2). Next, the optimization is conducted for the symmetric A and D layups. Compared to the uncoupled A optimum design, there is a further reduction in J of 15% for the symmetric A design and 3% for the symmetric D design. Again, it appears that lag bending–torsion coupling has negligible influence on reduction of vibratory hub loads and bending moments.

For the symmetric A optimum design, there is a reduction in all six 4/rev loads, compared to starting design A. The 4/rev longitudinal, lateral, and vertical forces are reduced by 20, 15, and 20%, respectively, and the 4/rev rolling, pitching, and yawing moments are reduced by about 30, 30, and 60%, respectively. The first five harmonics of the flap bending moment are reduced by 5, 15, 40, 10, and 60%, respectively; and the first, third, fourth, and fifth harmonics of the lag bending moments are reduced by 15, 5, 60, and 25%, respectively. However, the 6/rev harmonics of the flap and lag bending moments are increased by 20 and 25%, respectively, and the 2/rev lag bending moments increased by about 20%. Comparing the 4/rev loads and vibratory bending moments for cases 1–3 designs shows that the case 3 results give a compromise solution where vibratory hub loads are minimized without the significant increase in blade bending moments which occurred in case 1. In fact, for the case 3 optimum design, most harmonics of the root bending moments and the peak-to-peak value of the flap and lag bending moments are reduced by 11 and 14%, respectively.

The previous results show that by using elastic stiffness and flap bending–torsion coupling, it is possible to reduce both the vibratory hub loads and the vibratory bending moments. However, this reduction comes at the expense of lag mode stability; the lag mode damping is reduced by over 50%, from the starting design A value. The flap and torsion mode damping are increased by 5 and 30%, respectively.

For the symmetric A optimum design, the flap and lag stiffness are reduced at the root element by 15% each and increased at the four outboard elements, compared to the starting design. The torsion stiffness is increased at the inboard elements by about 10% and reduced at the outboard elements. The distribution of flap bending–torsion coupling for the design shows the largest coupling at the two inboard and tip elements and lesser coupling at elements 2 and 3. Again, the coupling is positive in sign throughout the blade–span. The distribution of the ply angle design variables that leads to these stiffnesses and couplings is shown in Figs. 9–11.

Figure 15 shows the variation of the torsion and flap response around the azimuth for the starting design A, uncoupled A, and symmetric A optimum designs. The symmetric A design causes a change in the tip torsion response of about 1–3 deg around the azimuth. The results in the form of closed loops in this figure are obtained at the design condition, $\mu = 0.3$. To get a physical feel for the amount of coupling induced for the optimum design, an aeroelastic analysis is performed for the starting and coupled designs in hover. Since there is no azimuthal variation in the response in hover, the hover results are a set of three points, for the starting design A, uncoupled A, and symmetric A designs. These points are also shown in Fig. 15. The nose-down twist obtained for this hover condition because of the flap bending–torsion coupling is 2.6 deg. Using the conventional definition of pitch–flap coupling ($\Delta\phi = -K_p\beta$), we obtain, for this hover condition, $K_p = 0.7$, which corresponds to a δ_3 angle of 35 deg ($K_p = \tan\delta_3$). Typically, helicopters have a δ_3 angle of the order of 20 deg. Figure 16 shows the lag response at the blade tip plotted with respect to the flap response. Clearly, the change in the lag response between the starting design and the optimum design is small compared to the change in torsion response.

The blade rotating frequencies for the first eight modes are shown in Table 2. Using these results in conjunction with those obtained by conducting a frequency sweep, a fan diagram is plotted as shown in Fig. 17. The frequencies for the starting design and the optimum design are always away from the in-

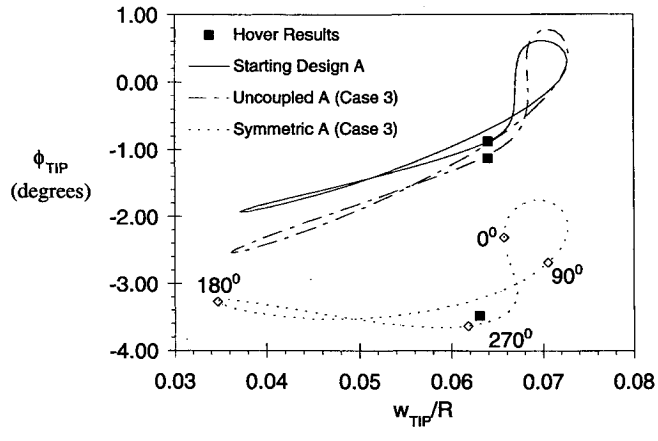

Fig. 15 Variation of blade tip torsion response with respect to tip flap response, for the initial and case 3 optimum designs.

teger multiples around the 1/rev speed. Also, the frequencies for the starting design and the optimum design are very close, the largest difference of about 2% occurs for the second lag frequency, which changes from 4.19 for the starting design to 4.28 for the optimum design. Therefore, reductions in the objective function obtained in this study are primarily because of changes in the blade response, and not because of changes in the blade frequencies.

Refined Aerodynamics

The previous results were obtained with quasisteady aerodynamics at $\mu = 0.3$. However, results obtained by performing the aeroelastic analysis with a free-wake inflow model[10] and unsteady aerodynamics[11] also show a reduction in the objective function at several forward speeds, even though the optimum design was obtained with a quasisteady aerodynamic model (Fig. 18).

Table 2 Rotating frequency for starting and optimum design

Mode	Starting design A, /rev	Symmetric A, case 3, /rev
First lag	0.72	0.69
First flap	1.14	1.13
Second flap	3.37	3.33
First torsion	3.62	3.61
Second lag	4.19	4.28
Third flap	7.37	7.30
Third lag	10.51	10.39
Second torsion	10.66	10.39

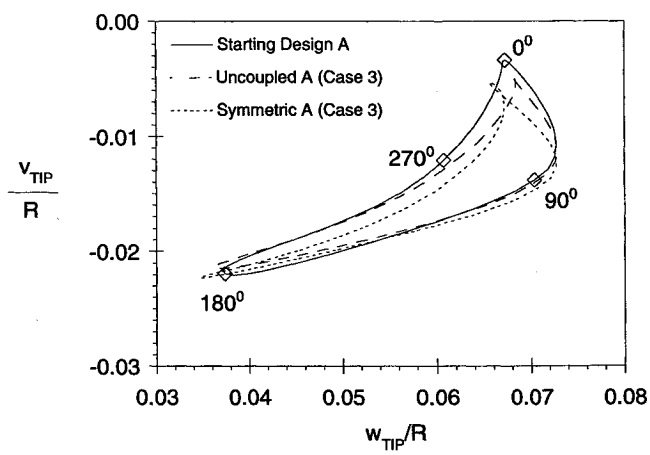

Fig. 16 Variation of blade tip lag response with respect to tip flap response, for the initial and case 3 optimum designs.

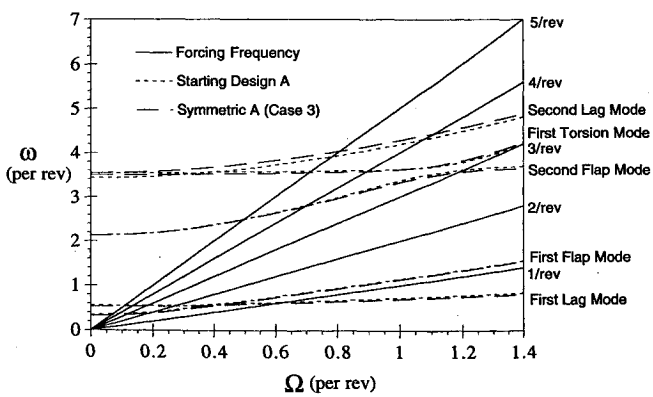

Fig. 17 Fan diagram for the starting A and the symmetric A optimum designs.

Infeasible Starting Design

The previous results showed that elastic stiffness and flap bending–torsion coupling can be tailored to reduce vibratory hub loads and bending moments. However, lag bending–torsion coupling was found to have a negligible effect on the optimum designs. It is well known that lag bending–torsion coupling has beneficial effects on aeroelastic stability, and since the stability constraint did not become active for the

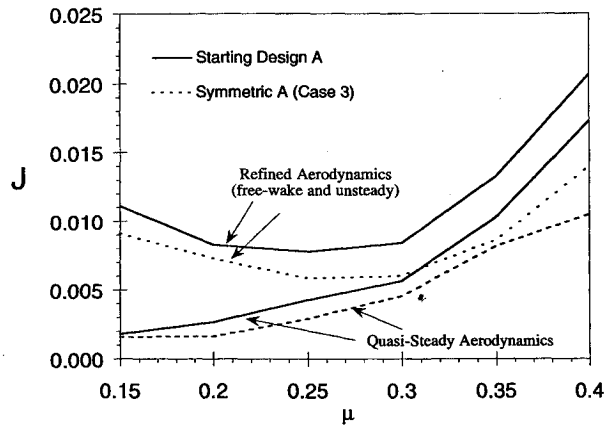

Fig. 18 Variation of objective function with forward speed for two cases: refined aerodynamics and quasisteady aerodynamics (optimum solution is calculated at $\mu = 0.3$ with quasisteady aerodynamics).

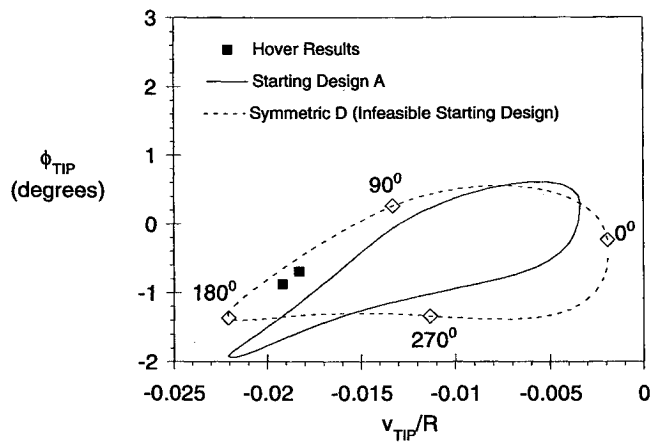

Fig. 19 Variation of blade tip torsion response with respect to tip lag response, for the initial and pitch-lag coupled optimum designs.

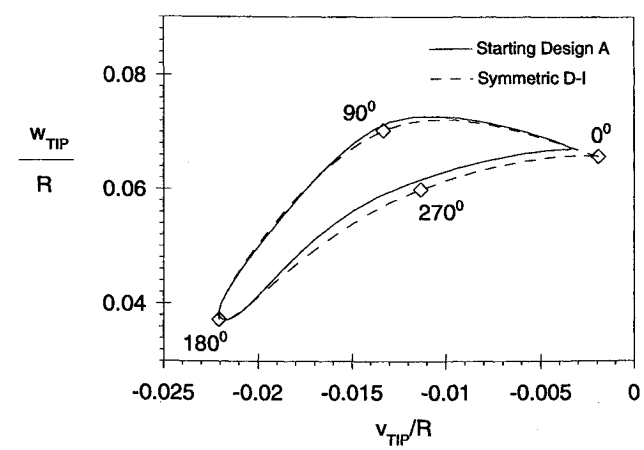

Fig. 20 Variation of blade tip flap response with respect to tip lag response, for the initial and pitch-lag coupled optimum designs.

results shown previously, lag bending–torsion coupling was not fully exploited. To make the stability constraint active during the optimization process, a margin of 3% is imposed on the lag mode damping. This makes starting design A an infeasible design ($\sigma_L = 0.0099 < 0.03$). The optimization is then performed using J (case 3) for the uncoupled A, symmetric A, and D layups.

The uncoupled A and symmetric A layups are unable to satisfy the 3% requirement on lag mode damping. Only the symmetric D layup (lag bending–torsion coupling) reaches an optimum design in the feasible region. This optimum design is called symmetric D-I. There is an increase in the lag mode damping of about 200% for the symmetric D-I design, compared to starting design A. This increase in lag mode damping comes at the expense of an increase in J of 13%. This increase in the objective function is because of an increase in both the vibratory hub loads and the vibratory bending moments as shown in Figs. 3 and 4 and Figs. 13 and 14, respectively. The elastic stiffness and coupling for the optimum design are shown in Figs. 5–8, respectively. The lag bending–torsion coupling $\bar{k}_{24}$ is negative and is distributed along the blade span. Note that positive $\bar{k}_{24}$ corresponds to negative pitch–lag coupling. The ply angle design variables corresponding to the optimum designs are shown in Figs. 9–11.

The blade tip torsion response is plotted with respect to the tip lag response in Fig. 19, for starting design A and the symmetric A optimum design. The change in twist because of the lag bending–torsion coupling is less than 1 deg around the azimuth. The two points on Fig. 19 represent the results in hover. Using the conventional definition of pitch–lag coupling ($\Delta\phi = -K_\zeta\zeta$), we obtain for the hover condition $K_\zeta = -0.18$, which corresponds to a δ_4 angle of -10 deg ($K_\zeta = \tan\delta_4$). The negative sign for the δ_4 angle shows negative pitch-lag coupling, which means that lag back-produces nose-up pitch motion. Figure 20 shows the variation of the tip flap response with respect to the tip lag response. It is clear that the change in the flap response between starting design A and the symmetric D optimum design is small compared to the change in the torsion response observed in Fig. 19.

Conclusions

Using an analytical formulation, rotor aeroelastic and sensitivity analyses are developed for a composite blade with a generic cross section. For the numerical study, a four-bladed soft in-plane hingeless rotor with a two-cell blade spar is investigated. Design variables are the ply angles of the laminated walls of the composite box–beam. The optimization problem consists of minimizing three different objective functions: 1) the vibratory hub loads alone J_v, 2) the vibratory bending moments at blade root alone J_d, and 3) a combination of vibratory hub loads and bending moments J. The following conclusions are drawn from this study:

1) When only J_v are minimized, the 4/rev loads are reduced by 20–70% compared to the starting design, because of elastic stiffness and flap bending–torsion coupling. However, the peak-to-peak flap and lag bending moments increase by 17 and 12%, respectively. The low vibration optimum rotor comes at the expense of reduced blade fatigue life.

2) When only J_d are minimized, the peak-to-peak flap and lag bending moments are reduced by 13 and 40% compared to the starting design, respectively. However, the 4/rev forces increase by about 10%.

3) The function J yields a reduction in the 4/rev loads of about 15–60%, and in the peak-to-peak flap and lag bending moment of 11 and 14%, respectively.

4) Even though the optimization is performed at $\mu = 0.3$ with quasisteady aerodynamics, reductions in both vibratory hub loads and bending moments are observed at other forward speeds, even when unsteady aerodynamics and free wake are used.

5) Starting from an initially infeasible design with a stability margin of 3% in the lag mode, the symmetric D layup (lag bending–torsion coupled) resulted in an increase in the lag mode damping of over 200% compared to the optimum solution for the uncoupled A blade. This increase in lag damping comes at the expense of an increase in the objective function of about 10%.

6) The maximum flap bending–torsion and the lag bending–torsion coupling obtained for the optimum designs are equivalent to a δ_3 angle (pitch–flap coupling) of 35 deg and a δ_4 angle (pitch–lag coupling) of -10 deg. Composites can be used to induce relatively large bending–torsion couplings in helicopter blades.

Acknowledgments

This research was supported by the Army Research Office, Contract DAAH04-93-G-001. Technical Monitors were Robert Singleton and Tom Doligalski.

References

[1]Panda, B., and Chopra, I., "Dynamics of Composite Rotor Blades in Forward Flight," *Vertica*, Vol. 11, Nos. 1–2, 1987, pp. 107–209.

[2]Smith, E. C., and Chopra, I., "Aeroelastic Response, Loads and Stability of a Composite Rotor in Forward Flight," *AIAA Journal*, Vol. 31, No. 7, 1993, pp. 1265–1274.

[3]Friedmann, P. P., "Helicopter Vibration Optimization Using Structural Optimization with Aeroelastic/Multidisciplinary Constraints," *Journal of Aircraft*, Vol. 28, No. 1, 1991, pp. 8–21.

[4]Ganguli, R., and Chopra, I., "Aeroelastic Optimization of a Helicopter Rotor with Composite Coupling," *Journal of Aircraft*, Vol. 32, No. 6, 1995, pp. 1326–1334.

[5]Ganguli, R., and Chopra, I., "Aeroelastic Optimization of a Helicopter Rotor with Two-Cell Composite Blades," *AIAA Journal*, Vol. 34, No. 4, 1996, pp. 835–854.

[6]Chandra, R., and Chopra, I., "Structural Behavior of Two-Cell Composite Rotor Blades with Elastic Couplings," *AIAA Journal*, Vol. 30, No. 12, 1992, pp. 2914–2924.

[7]Peters, D. A., and Cheng, Y. P., "Optimization of Rotor Blades for Combined Structural Performance and Aeroelastic Constraints," *Proceedings of the Symposium on Recent Advances in Multidisciplinary Analysis and Optimization*, NASA CP-3031, Pt. 1, 1988, pp. 163–180.

[8]Banerjee, D., and Santhakumaran, P., "Application of Numerical Optimization Methods in the Helicopter Industry," *Vertica*, Vol. 13, No. 1, 1989, pp. 17–42.

[9]Vanderplatts, G. N., "CONMIN—A Fortran Program for Constrained Function Minimization," User's Guide, NASA TMX 62282, Aug. 1973.

[10]Scully, M. P., "Computation of Helicopter Rotor Wake Geometry and Its Influence on Rotor Harmonic Airloads," Massachusetts Inst. of Technology, ASRL TR 178-1, Cambridge, MA, March 1975.

[11]Leishman, J. G., "Validation of Approximate Indicial Aerodynamic Functions for Two-Dimensional Subsonic Flow," *Journal of Aircraft*, Vol. 25, No. 10, 1988, pp. 914–922.